Acta Technica *62* (2017), No. 7A, 1339–1350

Interfacial shear strength analysis of fiber reinforced composite and metal bonding based on finite element method

Ya'nan Peng[1], Fan Mo[1*], Caiwen Mao[1], Mingcheng Bing[1]

Abstract. An interfacial shear strength analysis method based on finite element strategy is proposed to realize valid analysis of interfacial shear strength of fiber reinforced composite and metal bonding. Valid anisotropy of fiber reinforced composite and metal bonding interface and shear strength tensor of metal bonding surface can be obtained through finite element analysis (FEA) of volume element (shear strength) and it is approximated using finite element discrete equation and Galerkin discrete finite element combined with hole elasticity equation so as to obtain 3D space unstructured grid model of crack on the bonding contact surface. Through comparing example analysis and standard FEA result, the forecast result of the proposed algorithm is more accurate than that of algorithm in the existing literature.

Key words. Finite element, Grid model, fiber reinforced, Composite, shear strength, Metal bonding.

1. Introduction

In recent years, composite, especially fiber reinforced composite is more popular among automobile, aviation and packaging, etc. Fiber reinforced composite is lighter than traditional materials, like steel and aluminum, but it can provide similar shear strength performance of metal bonding surface [1∼2]. As fiber reinforced composite is applied more widely, it is necessary to understand the interfacial shear strength of these materials and metal bonding, how to react to specific load condition, and how the structure response changes with the change of bottom fiber reinforced composite

[1]School of Material Science and Engineering, Tongji University, ShangHai, China
*. Corresponding author

structure [3∼4].

Finite element method [5] (FEM) is an effective analysis tool. Using standard FEM to forecast the shear strength of metal bonding surface of fiber reinforced composite and requiring computing each fiber bundle of fiber reinforced composite requires huge quantity of commutating resources. Literature [6] develops the degree of freedom (DOF) of macroelement through static condensation or interpolation function. Literature [7] proposes fiber bundle expressed with grid and obtains matrix base through grid superposition. These methods provide rational result, but they need a lot of preprocessing time to build finite element grid of fiber bundle and matrix base system. Another FEA method is the grid that uses phase element to avoid material boundary. Literature [8] forecasts elasticity performance of fiber reinforced composite using phase element in the image processing. In nature, it is a geometric uniform element discretization method. Literature [9] analyzes the property of painting material in the element using volume fraction technology at the beginning. Literature [10] proposes a similar method and applies it to analysis of electromagnetic field. Literature [11] points out, sharp side can be improved with delicate grid at the cost of increasing the computation complexity.

The paper utilizes the material property of each integral point to correct local strain, and evaluates the 3D domain component of shear strength tensor of metal bonding surface using tensile modulus. Then, the paper formulates allowable shear for independent correction computation of extension clause, which can enhance the forecast precision of shear strength of shear isomerism.

2. Basic formulas

Firstly, the summation formula is used for repeating index and the summation is only expressed in 3D space. In addition, x_i refers to the *ith* space coordinate in the global coordinate system, and ξ_i refers to the *ith* space coordinate in reference element coordinate system.

2.1. Finite element method of structural mechanics

Firstly, according to strain deformation relationship, we get 3D linear elastic partial differential equation [12]:

$$\varepsilon_{ij} = \frac{1}{2}(u_{i,j} + u_{j,i})\,. \tag{1}$$

According to conservation theory of momentum:

$$-\sigma_{ij,j} - f_i + p\ddot{u}_i = 0\,. \tag{2}$$

Suppose Hokke's law meets the constitutive relation of three dimensions. We can make:

$$\sigma_{ij} = C_{ijkl}\varepsilon_{kl}\,. \tag{3}$$

In formula (1-3), u_i means *ith* component of displacement in the case of continuous density q, f_i represents internal pressure, σ_{ij} is local stress, ε_{ij} is local strain, and C_{ijkl} is shear strength tensor of anistropic four-order linear elastic metal bonding surface.

In Petrov-Galerkin FAM [13], geometric shape of material is discretized into element, and each element Ω^e is composed of N nodes. Thus, formula (2) is converted to weak form, and a system of linear algebraic equations later. For a static system, each element can write finite element equation:

$$K^e u^e = Q^e \,. \tag{4}$$

Hereinto, K^e is shear strength matrix on the metal bonding surface of an element, u^e is the node displacement vector of an element, Q^e is the vector of node force, and it is composed of force, reacting force, point load and surface force of an object.

Here, we are interested in shear strength matrix on the metal bonding surface of an element. The computational form is [14]:

$$K^e = \int_{\Omega^e} B^T C B d\Omega^e \,. \tag{5}$$

Hereinto, C is shear strength tensor on the 6×6 four-order metal bonding surface, B is matrix with the size of $6 \times 3N$, N is the number of node in FEA, and definition form of B is:

$$B(\xi_1, \xi_2, \xi_3) = [B_1, B_2, \cdots, B_N] \,. \tag{6}$$

In the formula, ψ_i^r is the derivative of the *rth* interpolation function for local space coordinate. It is expressed as:

$$\psi_i^r = \frac{\partial \psi^r}{\partial \xi_i} \,. \tag{7}$$

In addition, J_{ij}^{-1} is the component of inverse jacobian matrix, and the computational form is:

$$J_{ij}^{-1} = \frac{\partial \xi_j}{\partial x_i} \,. \tag{8}$$

2.2. Measurement of shear strength tensor on the metal bonding surface of material

For shear strength tensor on the metal bonding surface of C_{ijkl} component formed Hooke's law equation (3), it can be rewritten as 6×6 matrix C using stress σ and stain ε as below:

$$\sigma = C\varepsilon \,. \tag{9}$$

Hereinto,

$$\sigma = [\sigma_{11}, \sigma_{22}, \sigma_{33}, \sigma_{23}, \sigma_{13}, \sigma_{12}]^{\mathrm{T}} \,. \tag{10}$$

$$\varepsilon = [\varepsilon_{11}, \varepsilon_{22}, \varepsilon_{33}, 2\varepsilon_{23}, 2\varepsilon_{13}, 2\varepsilon_{12}]^{\mathrm{T}} \,. \tag{11}$$

Our goal is to determine average or homogenized $\bar{C}$ for shear strength, and it was composed of various heterogeneously arranged materials. In this case, the shear strength tensor $\bar{C}_{ijkl}$ on the metal bonding surface is supposed to be unknown, and the element of matrix $\bar{C}$ can be determined through FEM. To this end, strain state $\bar{\varepsilon}$ is applied to shear strength, and it can be used for computing average stress $\bar{\sigma}$. Then, we get element of matrix $\bar{C}$ through solving the equation set defined by formula (33).

Using six independent strain states respectively can determine one column of the given matrix $\bar{C}$ uniquely. For example, when average strain state $\bar{\varepsilon}_{11}$ is used for shear strength, other stresses are set up as 0, formula (33) can be simplified as a system of six algebra expression. The produced average stress value $\bar{\sigma}_{ij}$ is evaluated as below:

$$\bar{\sigma}_{ij} = \frac{1}{V}\int_{\Omega} \sigma_{ij} d\Omega \,. \tag{12}$$

Hereinto, V is total volume of shear strength. Six elements in the first column of C can be computed directly as:

$$\bar{C}_{11ij} = \frac{\bar{\sigma}_{ij}}{\bar{\varepsilon}_{11}} (i = 1, 2, 3, j \geq i) \,. \tag{13}$$

For repetition process with $\bar{\varepsilon}$ given, we can fill $\bar{C}$ totally through setting up single displacement on the boundary as 0 or non-zero.

In the research, periodicity is executed through displacement vector. Node displacement (u_d) on the target surface is equal to node displacement (u_s) on the source surface plus displacement vector c.

$$u_d = u_s + c \,. \tag{14}$$

The increased displacement vector c can include zero and non-zero value. It is related to average applied strain to $\bar{\varepsilon}$. For example,

$$\bar{\varepsilon} \approx \frac{1}{\Delta x}(u_d - u_s) \,. \tag{15}$$

Hereinto, Δx is the distance of node fro source surface to target surface. The increased displacement vector c can be computed:

$$c = (\Delta x)\bar{\varepsilon} \,. \tag{16}$$

There are six surfaces for cuboid element shown in Fig. 1, and each surface has a common vector parallel with three coordinate axes.

For area occupied by shear strength in Fig. $1(0 \leq x_1 \leq \Delta x_1; 0 \leq x_2 \leq \Delta x_2; 0 \leq x_3 \leq \Delta x_3)$, the node on the origin is fixed, we use $u\,(0, 0, 0) = 0$ to prevent rigid motion. In the formula, the second item on the right side of the latter four items is divided by 2. The reason is: in the model shown in Fig., for the selected three operative surfaces, the origin of three subcoordinate system is at the center of the plane. Thus, we select half of Δx_i.

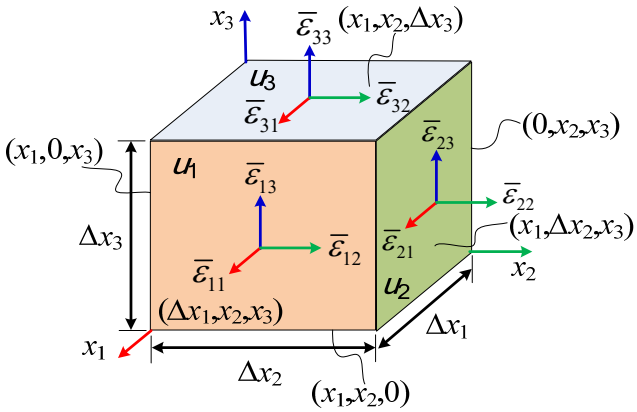

Fig. 1. A Cuboid that represents a volume unit

3. Discretization solution

3.1. Grid structure

Geometric element is used for dividing computational grid. Usually, tetrahedron is used for expressing matrix and triangle element represents fracture surface. To simplify narration, we use two-dimensional model grid, as is shown in Fig. 2. However, the designed method here is three-dimensional.

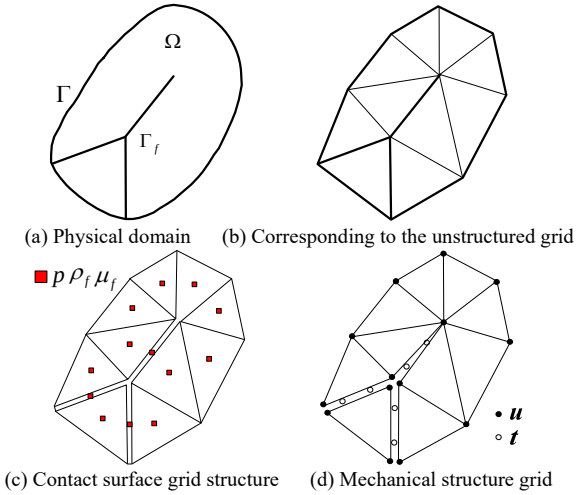

Fig. 2. Mesh of two dimensional model

In Fig. 2a, Ω is physical domain, Γ is external outline of model, and Γ_f is defined as fracture surface. In Fig. 2b, triangle expresses matrix, and bold line expresses fracture. The geometric grid is applicable to interface and mechanics problem of fiber reinforced composite and metal bonding. For the interface of fiber reinforced

composite and metal bonding, as is shown in Fig. 2c, the control volume is correlated to each element of grid. Pressure p, density ρ_f and viscosity μ_f are correlated to the cellular center. displacement is unknown, and u is correlated to the matrix peak. In Fig. 2d, different nodes express the displacement of each side of fracture. In addition, traction vector t is correlated to the surface of each fracture.

3.2. Bonding interface equation and discrete cracking model approximation

Finite element bonding interface equation is used for discretization. Based on both points approximating flux, the strength value of two adjacent controlled quantities can be expressed as pressure difference function:

$$Q_{ij} = \lambda T_{ij}(p_i - p_j)\,. \tag{17}$$

face of fiber reinforced composite and metal bonding can be defined as $\lambda = \rho_f/\mu_f$. Geometric transmission part is T_{ij}. Finite volume approximation scheme of backward Euler time and strength value is adopted, then the strength value equation (1) can be approximated:

$$\frac{p_{fi}^{n+l}\varphi_i^{n+1} - p_{fi}^{n}\varphi_i^{n}}{\Delta t}V_i = \sum_j Q_{ij} + q_i v_i\,. \tag{18}$$

Hereinto, V_i is volume of i, and time interval is Δt. Index $n+1$ and n corresponds to the current and next step.

3.3. Quasi-static hole elasticity equation

In the case of external boundary Γ and internal boundary Γ_f, the potential energy of interfacial bonding medium defined by formula (17-18)

$$\prod = \frac{1}{2}\int_\Omega \varepsilon : \Omega d\Omega - \int_\Omega \boldsymbol{u}\rho\boldsymbol{g}d\Omega - \int_\Gamma \boldsymbol{u}\bar{\boldsymbol{t}}d\Gamma - \int_{\Gamma_f} \boldsymbol{u}^{+}\bar{\boldsymbol{t}}_f^{+}d\Gamma - \int_{\Gamma_f} \boldsymbol{u}^{-}\bar{\boldsymbol{t}}_f^{-}d\Gamma\,. \tag{19}$$

Hereinto, $\bar{\boldsymbol{t}}$ is the total transaction vector on the boundary Γ. Total transaction $\bar{\boldsymbol{t}}_f^{-}$ and $\bar{\boldsymbol{t}}_f^{+}$ is on the opposite side of fracture interface. Based on continuity condition, it is got:

$$\prod = \frac{1}{2}\int_\Omega \varepsilon : \Omega d\Omega - \int_\Omega \boldsymbol{u}\rho\boldsymbol{g}d\Omega - \int_\Gamma \boldsymbol{u}\bar{\boldsymbol{t}}d\Gamma - \int_{\Gamma_f} (\boldsymbol{u}^{+} - \boldsymbol{u}^{-})\bar{\boldsymbol{t}}_f d\Gamma\,. \tag{20}$$

In the formula, $\bar{\boldsymbol{t}}_f$ combines the impact of interfacial pressure p and Terzaghi effective effect σ' of fiber reinforced composite and metal bonding.

$$\bar{\boldsymbol{t}}_f = -\sigma\boldsymbol{n} = -(\sigma' - \boldsymbol{I}p)\boldsymbol{n} = t_N\boldsymbol{n} + t_T\boldsymbol{\tau} + p\boldsymbol{n}\,. \tag{21}$$

Gap function g can be expressed as displacement function:

$$g = u^+ - u^- = (g_N, g_T)\,. \tag{22}$$

Thus, we can get the following potential energy function:

$$\prod = \frac{1}{2}\int_\Omega \varepsilon : \sigma d\Omega - \int_\Omega \boldsymbol{u}\rho\boldsymbol{g}d\Omega - \int_\Gamma \boldsymbol{u}\bar{\boldsymbol{t}}d\Gamma - \int_{\Gamma_f} g_n p d\Gamma - (\int_{\Gamma_f} g_N t_N + g_T t_T)d\Gamma\,. \tag{23}$$

The minimal potential energy is solved using differential:

$$\begin{aligned}\delta\prod =& \frac{1}{2}\int_\Omega \delta\varepsilon : \sigma d\Omega - \int_\Omega \delta\boldsymbol{u}\rho\boldsymbol{g}d\Omega - \int_\Gamma \delta\boldsymbol{u}\bar{\boldsymbol{t}}d\Gamma \\ & - \int_{\Gamma_f} \delta g_n p d\Gamma - (\int_{\Gamma_f} \delta g_N t_N + \delta g_T t_T)d\Gamma\,.\end{aligned} \tag{24}$$

We make finite element approximation based on node, and the displacement can be defined as:

$$\boldsymbol{u}(\xi) \approx \sum_a N_a(\xi)\boldsymbol{u}_a\,. \tag{25}$$

Hereinto, $\boldsymbol{u}_a$ is node displacement value, and N_a is shape function. Then, the gap function of fracture on the bonding contact surface can be defined as:

$$g(\xi) = \boldsymbol{u}^+(\xi) - \boldsymbol{u}^-(\xi) \approx \sum_a N_a(\xi)(\boldsymbol{u}_a^+ - \boldsymbol{u}_a^-) = \sum_a N_a g_a\,. \tag{26}$$

Hereinto, $\boldsymbol{u}^+$ and $\boldsymbol{u}^-$ correspond to double-side displacement of fracture. The surface is discretized as $\Gamma_f = \cup_e \Gamma_{f,e}$, then the integral form of fracture surface is:

$$\begin{aligned}&\int_{\Gamma_f} \delta g_N p d\Gamma - \int_{\Gamma_f} (\delta g_N t_N + \delta g_T t_T)d\Gamma \approx \sum_e \times \int_{\Gamma_{f,e}} \sum_a \delta(g_N)_a N_a p d\Gamma \\ &- \sum_e \times \int_{\Gamma_{f,e}} (\sum_a \delta(g_N)_a N_a t_N + \sum_a \delta(g_T)_a N_a t_T)d\Gamma\,.\end{aligned} \tag{27}$$

Traction vector (t_N, t_T) is shown as before. On the ideal condition, based on Kuhn-Tucker theorem, the friction law is got as below:

$$\begin{cases} t_N \geq 0, g_N \geq 0, t_N g_N = 0, \dot{g}_T(\xi) - \eta\dfrac{\partial\Phi}{\partial t_T} = 0 \\ \Phi = |t_T| - \mathcal{F}(t_N) \leq 0, \eta \geq 0, \Phi \leq 0, \eta\Phi = 0 \end{cases} \tag{28}$$

Obviously, when $\Phi = 0$, slippage occurs; when $\Phi < 0$ and $\dot{g}_T = 0$, adhesion appears. Thus, the Kuhn-Tucker constraint and adhesion/slippage rule of can be

replaced with:

$$\begin{cases} \dot{g}_T(\xi) - \eta \dfrac{\partial}{\partial t_T}\Phi = \dfrac{1}{\varepsilon_T}\dot{t}_T \\ t_N = \varepsilon_N g_N, \eta \geq 0, \Phi \leq 0, \eta\Phi = 0 \end{cases} \tag{29}$$

Hereinto, $\varepsilon_N \gg 1$, $\varepsilon_T \gg 1$ are penalty factors. Here, ε_N acts as shear strength of the artificial metal bonding surface on the fracture surface. According to the above formula, it is known, when $g_N > 0$, penetration occurs.

During deformation, contact surface is directly proportional to the applied force. Thus, the normal contact surface meets the following equation:

$$\mathcal{N}(g_N) = \frac{k_n g_0}{g_0 \cdot g_N} g_N \,. \tag{30}$$

Hereinto, is shear strength on the initial normal metal bonding surface. In "ideal" case, we can consider the surface roughness contact problem as below:

$$\begin{cases} t_N = \mathcal{N}(g_N), g_N \leq g_0 \\ \dot{g}_T - \eta \dfrac{\partial}{\partial t_T}\Phi = \dfrac{1}{\varepsilon_T} i_T \\ \eta \geq 0, \Phi \leq 0, \eta\Phi = 0 \end{cases} \tag{31}$$

Traction vector is evaluated using return mapping algorithm, and the form is:

$$\begin{cases} t_N^{n+1} = N(g_N^{n+1}) \\ t_T^{trial} = t_T^n + \varepsilon_T(g_T^{n+1} - g_T^n) \\ \Phi^{trial} = |t_T^{trial}| - \mathcal{F}(t_N^{n+1}) \\ t_T^{n+1} = t_T^{trial}, if \Phi^{trial} \leq 0 \\ |t_T^{n+1}| = \mathcal{F}(t_N^{n+1}), if\ \Phi^{trial} > 0 \end{cases} \tag{32}$$

Hereinto, the subscript $n+1$ and n are the current and the previous step.

4. Experimental analysis

4.1. Interfacial bonding layer

The studied fiber reinforced composite is called 2/2 plain weave in this paper. Hereinto, a strand will pass through two strands and go beyond two strands. In this model, an offset in each column creates a "stair-step" model; sets up $h_f = h_w =$ 0.15mm and $a_f = a_w = 1.5$mm

Table 1 shows contrast between experimental result obtained using FEM combined with different measurements methods in Chapter 3 and analysis result of Literature [15.]

Table 1. Parameter setting

Parameter	Fiber bundle (carbon/bakelite)	Matrix (bakelite)
E_{11}(GPa)	137	3.2
$E_{22} = E_{33}$(GPa)	9.57	3.2
$G_{12} = G_{13}$(GPa)	4.74	1.19
G_{23}(GPa)	3.23	1.19
$v_{12} = v_{13}$	0.31	0.35
v_{23}	0.45	0.35

Table 2. Calculated values of stiffness characteristics of plain weave finite element analysis

Parameter	ASE	B-FEA	TMC- FEA	STC- FEA (Orig.)	STC- FEA (Adj.)	Literature [15]
E_{11}(GPa)	44.8	44.9	43.2	43.1	47.2	49.38
E_{22}(GPa)	44.8	44.9	43.2	43.1	47.2	49.38
E_{33}(GPa)	8.13	8.05	7.80	7.78	8.33	n/a
G_{12}(GPa)	2.49	2.45	2.30	2.44	2.57	n/a
G_{13}(GPa)	2.49	2.45	2.30	2.44	2.57	n/a
G_{23}(GPa)	3.23	3.23	3.15	3.20	3.46	2.36
v_{12}	0.46	0.46	0.46	0.46	0.49	n/a
v_{13}	0.46	0.46	0.46	0.46	0.49	n/a
v_{23}	0.09	0.09	0.08	0.08	0.09	0.06

STC-FEA result of the 5th column in Table 2 shows that the tensile modulus after adjustment has better consistency with the experimental result. For STC-FEA, the computational result of parameter E_{11} and E_{12} in adjustment mode is superior to the operation result in original mode. For parameter G_{12}, the result in original mode is more accurate to that in adjustment mode. However, it is within the expectation, because all the input shear modulus increases by 10%. Similar research can be completed through changing volume fraction and several geometric parameters.

4.2. Research on fiber morphology parameter

The last research is volume fraction computation of different fiber bundles. It has the ability of controlling geometric shape of chain within shear strength, so the volume fraction V_f of composite can be changed simply. STC-FEA code written with matlab is used for analyzing codes and the volume fraction change of shear strength composite layer is measured. The geometric shape of the whole element is set up as: $a_{RVE} = 1.20$ mm and $h_{RVE} = 0.10$ mm. Chain width a_f and a_w is set up as 0.48mm, and the fiber thickness h_f and h_w can be computed:

$$h_f = h_w \approx \frac{\pi a_{RVE} h_{RVE} V_f}{4 a_f} \,. \tag{33}$$

In the research, the volume fraction of 25 fiber reinforced composites ranges from 0.25 to 0.50. The volume fraction advantage of FEM is analyzed using STC-FEA grid element of 35,152 lines. See Fig. 3 for experimental result.

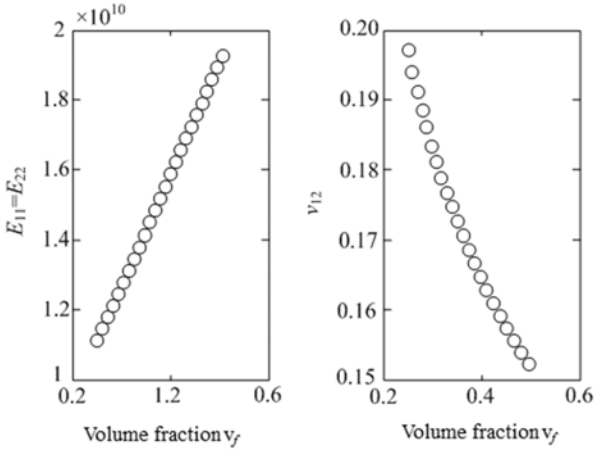

Fig. 3. Experimental data of volume fraction based on STC-finite element analysis

According to the result of Fig. 3, it is known, for two shear strength constants on the engineering metal bonding surface selected from research on volume fraction of plain weave fiber reinforced composite, the plain weave fiber reinforced composite meets $E_{11}(V_f) = E_{22}(V_f)$. Generally speaking, the fiber direction of tensile modulus $E_{11}(V_f)$ is nearly linear. It is basically identical to the analysis result of the existing literatures.

5. Conclusion

The paper proposes an interfacial shear strength analysis method based on finite element strategy. Valid anisotropy of fiber reinforced composite and metal bonding interface and shear strength tensor of metal bonding surface can be obtained through finite element analysis (FEA) of volume element (shear strength) and it is approximated using finite element discrete equation and Galerkin discrete finite element combined with hole elasticity equation. Through example analysis, it is seen that the forecast result of the proposed algorithm is more accurate than the algorithm in the existing literature. The purpose of such design is to allow multiple materials stored in a single element, which eliminates the processing time required by the complicated geometric shape. In the research, the expandable coupling items are ignored, which is to be studied in the future.

References

[1] J. W. Chan, Y. Y. Zhang, and K. E. Uhrich: *Amphiphilic Macromolecule Self-*

Assembled Monolayers Suppress Smooth Muscle Cell Proliferation, Bioconjugate Chemistry *26* (2015), No. 7, 1359–1369.

[2] J. W. Chan, Y. Y. Zhang, and K. E. Uhrich: *Amphiphilic Macromolecule Self-Assembled Monolayers Suppress Smooth Muscle Cell Proliferation*, Bioconjugate Chemistry *26* (2015), No. 7, 1359–1369.

[3] M. P. Malarkodi, N. Arunkumar, N., V. Venkataraman: *Gabor wavelet based approach for face recognition.* International Journal of Applied Engineering Research *8* (2013), No. 15, 1831–1840.

[4] L. R. Stephygraph, N. Arunkumar: *Brain-actuated wireless mobile robot control through an adaptive human-machine interface.* Advances in Intelligent Systems and Computing *397* (2016), 537–549.

[5] W. S. Pan, S. Z. Chen, Z. Y. Feng:*Investigating the Collaborative Intention and Semantic Structure among Co-occurring Tags using Graph Theory.* International Enterprise Distributed Object Computing Conference, IEEE, Beijing (2012), 190–195.

[6] N. Arunkumar, S. Jayalalitha, S. Dinesh, A. Venugopal, D. Sekar:*Sample entropy based ayurvedic pulse diagnosis for diabetics.* IEEE-International Conference on Advances in Engineering, Science and Management, ICAESM-2012, art. no. 6215973 (2012) , 61–62.

[7] N. Arunkumar, K. Ramkumar, S. Hema, A. Nithya, P. Prakash, V. Kirthika:*Fuzzy Lyapunov exponent based onset detection of the epileptic seizures.* 2013 IEEE Conference on Information and Communication Technologies, ICT 2013, art. no. 6558185 (2013), 701–706.

[8] J. J. Faig, A. Moretti, L. B. Joseph, Y. Y. Zhang, M. J. Nova, K. Smith, and K. E. Uhrich: *Biodegradable Kojic Acid-Based Polymers: Controlled Delivery of Bioactives for Melanogenesis Inhibition*, Biomacromolecules *18* (2017), No. 2, 363–373.

[9] N. Arunkumar, V. Venkataraman, Thivyashree, Lavanya:*A moving window approximate entropy based neural network for detecting the onset of epileptic seizures.* International Journal of Applied Engineering Research *8* (2013), No. 15, 1841–1847.

[10] Y. J. Zhao, L. Wang, H. J. Wang, and C. J. Liu: *Minimum Rate Sampling and Spectrum Blind Reconstruction in Random Equivalent Sampling.* Circuits Systems and Signal Processing *34* (2015), No. 8, 2667–2680.

Received May 7, 2017